Results in Physics 16 (2020) 103014

Contents lists available at ScienceDirect

Results in Physics

journal homepage: www.elsevier.com/locate/rinp

Heat treatment effect on the structural, morphological, and optical properties of plasma polymerized furan-2-carbaldehyde thin films

Humayun Kabir[a,b,c,*], Rahima Nasrin[c,d], M. Mahbubur Rahman[a,e], A.H. Bhuiyan[c]

[a] Department of Physics, Jahangirnagar University, Savar, Dhaka 1342, Bangladesh
[b] School of Engineering, RMIT University, Bundoora, Victoria 3083, Australia
[c] Department of Physics, Bangladesh University of Engineering and Technology, Dhaka 1000, Bangladesh
[d] Department of Physics, University of Barisal, Barisal 8200, Bangladesh
[e] Discipline of Chemistry and Physics College of Science, Health, Engineering and Education, Murdoch University, Perth, WA 6150, Australia

ARTICLE INFO

Keywords:
Furan-2-carbaldehyde
Glass substrates
Plasma polymerization technique
Fourier transform infrared spectroscopy
Heat treatment
Direct band-gap

ABSTRACT

The furan-2-carbaldehyde (PPFCD) amorphous polymer thin films, with several thicknesses, were deposited onto glass substrates using a glow discharge of monomer FCD at ordinary room temperature *via* plasma polymerization technique. The structural, morphological, and optical characteristics of the as synthesised PPFCD amorphous films were studied as a function of temperature *via* X-ray diffraction (XRD), Fourier transform infrared (FTIR) spectroscopy, scanning electron microscopy (SEM), energy dispersive X-ray analysis (EDX), and ultraviolet-visible (UV–Vis) absorption spectroscopy. The amorphous nature of the thin films was ascertained in both as-synthesised and heat treated states using the XRD studies. The SEM micrographs display homogeneous and fracture free surface of PPFCD films and no remarkable variation in the surface morphology of the as synthesised films was detected owing to the heat treatment procedure. However, the EDX, and FTIR analysis represented some structural rearrangement originated from the heat treatment of the PPFCD thin films. The analysis of the UV–Vis absorption spectroscopy revealed that the absorbance of the films depend on the films thickness and the temperature of the heat treatment. The optical band-gaps of PPFCD amorphous films were found to be significantly decreased with the gradual rise in heat treatment temperature.

Introduction

Plasma polymerization (PP) technique has been used as a useful tool over the past few decades, to polymerize organic vapours at low temperatures using plasma enhancement. This method is also broadly utilized to deposit thin polymer films from various organic compounds called monomer [1–3]. The physical structure and various characteristic of plasma polymer thin films depend upon several parameters, for example, discharge power, monomer flow rate, substrate temperature, and steady-state pressure in the reactor chamber. The PP organic thin films have found extensive applications in thin film diodes, transistors and lens, switching, photovoltaic and optoelectronics devices, membrane separation, sensors, rechargeable batteries, and dielectric [4–9]. Thus, preparation of high quality polymer thin films using an appropriate technique, for a variety of monumental applications, always remains in the hot spot. Consequently, study of structural, electronic, electrical, and optical characteristics of PP organic polymer films as potential advanced materials have acquired distinct attention to the materials and solid state scientists [10].

Modification of various properties of PP thin films using aging and heat treatment procedures, may offer amazing applications in several devices fabrications. Since PP thin films possess substantial content of free radicals, oxidation, bonding of radicals with polymer chains, so the influence of aging as well as heat treatment on a PP thin films under ambient environments should be taken into account for their stability in appropriate application [11,12]. A large number techniques has been successfully utilized to synthesize functional polymer thin films such as, thermal evaporation [13], ion beam sputtering [14], RF magnetron sputtering [15], atomic layer deposition [16], chemical vapour deposition (CVD) [17], plasma enhanced chemical vapour deposition [18], plasma polymerization [19–22], sol–gel [23], and pulsed plasma CVD [24]. Among the existing methods, plasma polymerization is very popular because it can produce very thin films and nearly all kinds of organic vapours can be utilized to fabricate polymer thin films. In addition, films produced using PP method yields outstanding adhesion to the substrates, remarkable thermal and chemical stability, highly cross-

* Corresponding author.
E-mail address: s3760684@student.rmit.edu.au (H. Kabir).

https://doi.org/10.1016/j.rinp.2020.103014
Received 23 October 2019; Received in revised form 11 February 2020; Accepted 14 February 2020
Available online 17 February 2020

linked, as well as fracture free characters [19,25].

PP thin films have widely explored to comprehend their structural, optical, electrical and thermal characteristics and to seek out their prospective applications in science and technology [26–33]. For instance, Afroze et al. [34] observed the influence of heat treatment temperature on the structural, morphological, and optical properties of plasma deposited 2-(diethylamino) ethylmethacrylate thin films synthesized using PP technique, and reported that the energy band-gaps of the films were gradually reduced due to the heat treatment procedure. Authors also reported that the band-gap engineering of these films play important role in device applications. The aging and heat treatment effect on several properties including structure, thermal, and optical properties of PP 2, 6-diethylaniline (PPDEA) thin films studied by Matin et al. [35], indicating the structural rearrangements in PPDEA films taken place on account of the heat treatment process. They also reported that the energy band-gaps of PPDEA films were significantly altered by the heat treatment, while those were not observed due to aging. Moreover, other optical parameters, for instance, Urbach energy (E_u), steepness parameter (σ) and extinction coefficient (k) were also strongly influenced by the heat treatment. In another study, Nasrin et al. [36] reported the thickness and heat treatment effect on PP *n*-butyl methacrylate (nBMA) thin films. Their obtained result indicated that structural alteration was occurred due to heat treatment. Besides, optical band-gaps and Urbach energy were found to be reduced because of the heat treatment and these tailoring of the band-gaps and other optical parameters suggested that the PPnBMA films can be considered as a potential prospect for surface protective cover in optoelectronic devices. In a more recent work, Humayun et al. [37] studied the influence of aging on 2-Furancarboxaldehyde (PPFCD) thin films thin films, and found that the optical properties of the as synthesised PPFCD thin films has been altered due to the aging effect. The optical studies of Iodine doped PPDEA thin films showed a remarkable reduction in the energy band-gap with subsequent enhancement of Iodine-content [38]. The influence of heat treatment on the optical characteristics of PP vinylene carbonate (VC) thin films indicated that the optical absorption of PPVC films was progressively increased, on the contrary the optical band-gap was reduced owing to the increase in heat treatment temperature [39]. They also reported that by choosing an appropriate heat treatment temperature the PPVC films may work as an active material for fabrication of organic thin films to be utilized in electronic and optoelectronic devices. Till now, comprehensive reviews on the synthesis mechanism and heat treatment effects on different properties of PPFCD thin films are scanty. In this work, furan-2-carbaldehyde (FCD), a derivative of furan was chosen as the monomer and was expected to generate PPFCD polymer thin films with interesting properties and influence of heat treatment on structural, morphological, thermal, and optical behaviours of PPFCD thin films was thoroughly analysed.

Experimental

Synthesis and thickness measurement

The analytical grade chemical reagents, such as furan-2-carbaldehyde (FCD) in liquid form, were purchased from Sigma Aldrich, UK, and were used as received. Fig. 1 shows the chemical structure of FCD, while its common physical and chemical properties are presented in Table 1.

Chemically and ultrasonically cleaned glass slides (Sail Brand, China) with dimensions (25.4 × 76.2 × 1.2) mm^3 were used as substrates. The FCD vapour was inserted into the glow discharge reactor

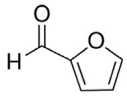

Fig. 1. The chemical structure of furan-2-carbaldehyde.

Table 1
General properties of furan-2-carbaldehyde.

Commercial Name	Furfural
Commercial name	Furfural
IUPAC name	2-furaldehyde
Form	Clear liquid
Colour	Colourless oil
Molecular formula	$C_5H_4O_2$
Chemical formula	OC_4H_3CHO
Molecular weight	96.0841 g/mol
Density	1.160 g/cm^3
Freezing point	−37 °C
Boiling point	162 °C
Vapour pressure	13.5 mm Hg (55 °C)
Flash point	62 °C
Refractive index	1.5235

system at a steady rate of 20 cm^3/min with the help of a flow meter. The glow discharge system is a cpapacitively coupled reactor consisting of two circular stainless steel parallel plate electrodes with a diameter and a thickness of 9.0 and 0.1 cm, respectively, placed approximately 4.0 cm away from each other. A sketch of PP apparatus arrangement is depicted in Fig. 2 [40]. First of all, a rotary pump (Vacuubrand GMBH & Co., Germany) were employed to evacuate the chamber of the reactor, and then a base pressure of approximately 1.33 Pa was maintained in the vacuum chamber. Then, a glow discharge plasma was created via a step up transformer at all around the glass substrates, placed on the lower plate of the electrode. The electrode was operated at a power range between 30 and 50 W at line frequency of 50 Hz. A constant pressure of around 13.3 Pa was maintained in the reactor chamber of the PP system during the film deposition process. The deposition time (t) was changed in between 30 and 90 min to fabricate satisfactory thicknesses of PPFCD thin films, and then the multiple-beam interferometric technique [41] was utilized to determine the thickness, d of the as synthesised PPFCD thin films,

$$d = \frac{\lambda q}{p} \tag{1}$$

where λ (= 5893 Å), q, and p is the wavelength of the used light source, step height, and width of the Fizeau fringes, respectively. A traveling microscope was utilized to measure the values of q and p. The fringes observed from PPFCD films are shown in Fig. 3. Set of graphs plotted between d and t at several powers like 30, 40, and 50 W were presented in Fig. 4 which demonstrated the growth kinetics of PPFCD films. Fig. 4 indicated that the generated plasma around the electrodes was not satisfactory to achieve suitable film thickness at the power of 30 W, contrariwise the production of plasma is very high at a power of 50 W, resulting an unhurried fabrication of PPFCD films. However, it was found that appropriate PP of FCD was taken place at a power of 40 W. Consequently, electrode power 40 W was used to obtain appropriate thicknesses of PPFCD thin films for different measurements.

Heat treatment of PPFCD thin films

The as-synthesised PPFCD thin films with several thicknesses were heat treated at three temperatures, such as 373, 473, and 573 K in air environment for 2.0 h using a programmable furnace at a heating rate of 5.0 K/min. In contrast, for FTIR study, PPFCD powders were scraped from the circularly shaped electrodes and then heat treated at 473, and 573 K in air for 2.0 h using the same furnace and same conditions. The temperatures were selected from 373 to 573 K because from thermal analyses it was found that the PPFCD film films are thermally stable from room temperature to about 600 K.

Characterization

The Equinox 3000 (Inel 405 45,410 Artenay, France) powder X-ray

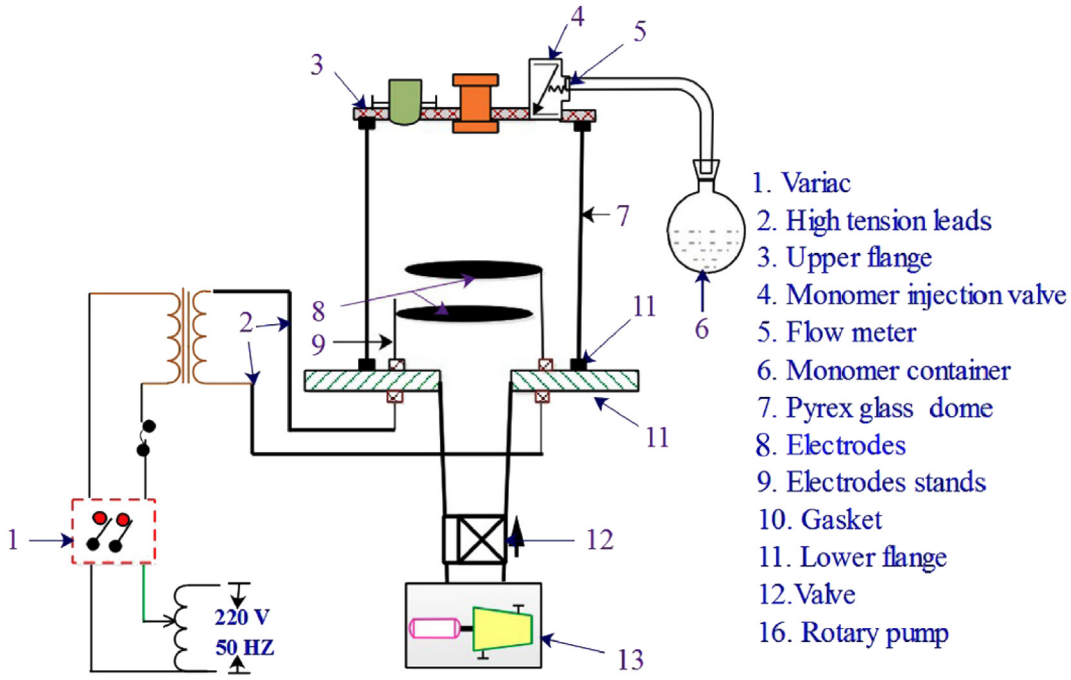

Fig. 2. The Schematic diagram of Plasma polymerization set up.

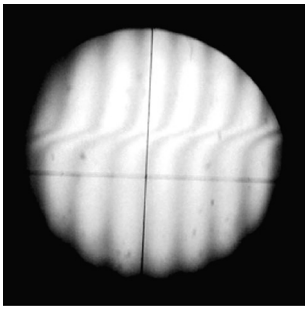

Fig. 3. The Fizeau fringe pattern of PPFCD thin film.

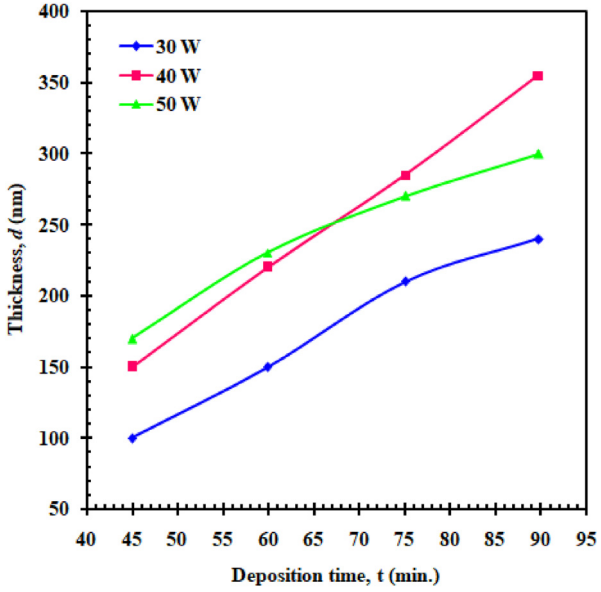

Fig. 4. Variation of *d* with *t* for the PPFCD thin films at different plasma powers.

diffractometer (XRD) were utilized to analysis the crystal structure of the PPFCD thin films in the 2θ range of 10 to 80° in steps of 0.03°, with Cu-K_α radiation. The XRD machine was operated at an operating voltage of 35 kV and a current of 25 mA. The recorded XRD scan data were analysed using the Match computer software. The FTIR spectra of the FCD, as deposited, and heat treated PPFCD films were taken in transmittance (%) mode to comprehend the chemical structure of the films using a dual beam FTIR spectrophotometer (SHIMADZU FTIR-8900 spectrophotometer, Japan) at the wavenumber range between 400 and 4000 cm^{-1}. In order to acquire the FTIR spectra of the monomer, FCD, a droplet of liquid FCD was placed in a KBr measuring cell while in the case of PPFCD, a ratio of 2:100 of the sample and KBr in the form of pellets were used. The scanning electron micrographs of the PPFCD thin film surface was taken using an SEM machine coupled with an EDX measuring system (Inspect F50, EFI, Netherlands) operated at a voltage of 20 kV. Prior to this, a thin layer of gold was coated onto PPFCD thin films via gold sputtering to get off the charging effect during operation of the SEM. The UV–Vis spectroscopic analysis of PPFCD films were carried out with the help of a dual beam UV–Vis spectrophotometer at room temperature in the absorbance mode between 270 and 800 nm wavelength range. For TGA and DTA measurements, the PPFCD films were grazed off from the substrate and scans of the films were carried out at a heating rate of 10 K/min under N_2 gas flow from room temperature, 300 K to 873 K via a computer controlled TG/DTA 6300 system (Seiko Instruments Inc., Japan).

Results and discussion

Thermal analysis

The TGA, and DTA analysis of as-deposited PPFCD thin films, in the temperature range 300–900 K in steps of 100 K, is shown in Fig. 5. The represented TGA trace indicates that mass of the films is gradually reduced at different stages due to heating. The TGA curve reveals that in the low temperature region, 360 K, the initial mass loss is 3.5%. This mass loss phenomenon may be associated with the exclusion of absorbed surface water. It is further believed that at low temperature region the mass loss is not arising due to the structural modifications of the PPFCD thin films. The corresponding DTA trace shows a tiny peak

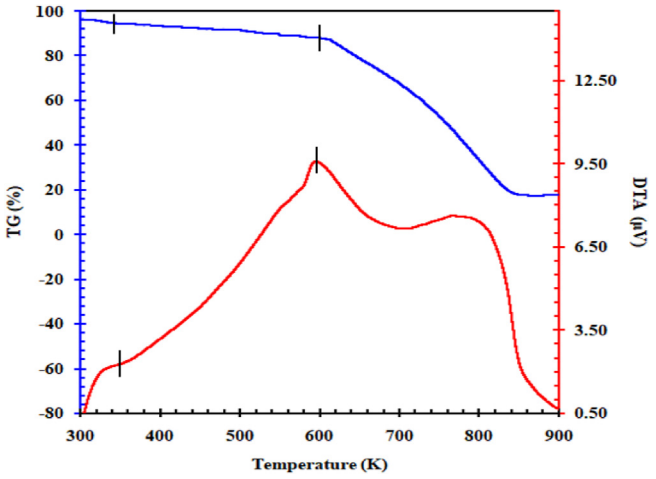

Fig. 5. The TGA and DTA traces of as-deposited PPFCD in air environment.

originated from the evolution of absorbed water from PPFCD thin film surface. After this small peak, a well-defined plateau region up to 600 K was detected. This distinct plateau suggests that the PPFDH films are stable up to 600 K. Over 600 K, in the TGA trace, an abrupt mass loss is believed to be emerged from the polymer decompositions, *i.e.*, evolution of H, CO, and CO_2 by the PPFCD films. The corresponding the DTA curve represents an exothermic broad band together with a maxima centred at 600 K demonstrating a successive alternation of the film behaviours. A similar trend of weight loss behaviour of poly methyl methacrylate (PMMA) films was reported by Kaniappan et al. [42]. Authors also demonstrated that the major weight loss of PMMA films occurred in the temperature range of 520 to 680 K. Afroze et al. also reported that PPDEAEMA films were stable up to 550 K and prime weight loss occurred between 500 and 860 K [34]. In our study, key weight loss of PPFCD films was observed between the temperature range of 550 and 760 K.

Structural analysis of PPFCD films

XRD analysis

The XRD measurements of as-synthesised (at 298 K) and heat treated (at 373, 473 and 573 K) PPFCD thin films having thickness

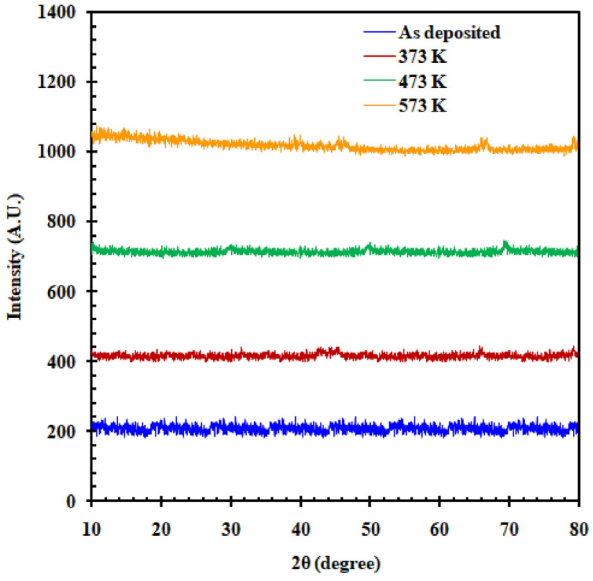

Fig. 6. The XRD pattern of as-deposited and heat treated PPFCD thin films.

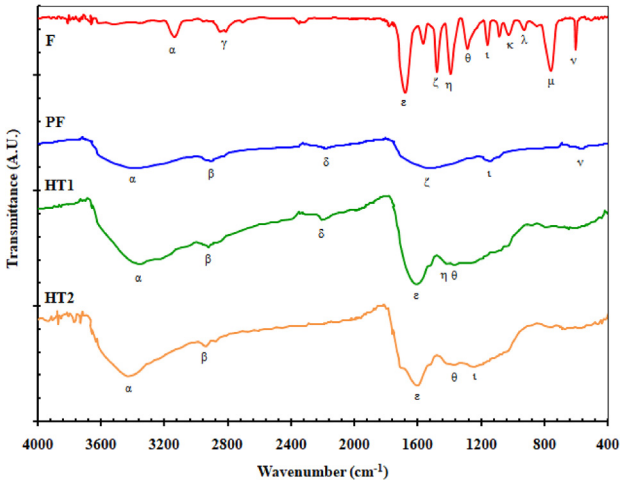

Fig. 7. The FTIR spectra of the FCD (spectrum F), as deposited PPFCD (spectrum PF) and PPFCD heat treated at 473 K (spectrum HT1), and at 573 K (spectrum HT2) samples.

230 nm are depicted in Fig. 6. It can be seen from Fig. 6 that there is no well-defined Bragg peaks in the XRD patterns. Non-existence of distinct crystalline peaks illustrated that both as-deposited and heat treated PPFCD films are either in amorphous state or have very tiny crystallites undetectable by the XRD measurements. Further inspection also indicated that there is no heating effect on the amorphous characteristics of the PPFCD thin films

FTIR spectroscopy investigation

The FTIR spectra, as a function of wavenumber in the case of FCD, as-synthesised and heat treated PPFCD films are illustrated in Fig. 7. The FTIR spectra of FCD, as synthesised as well as heat treated PPFCD samples are identified respectively by F, PF, HT1 and HT2. The FTIR spectra of these films showed the existence and transformations of multifarious functional groups in the film sample surfaces.

In the spectrum F, a broad band appeared at 3450–3150 cm^{-1} pointing out the existence of −OH stretching band which yields the key features of the band skeletons. As −OH is absent in the original chemical structure of the FCD, we believe that the −OH groups in F is due to the disclosure of monomer structure to the air. The −OH stretching band has been also seen in PF, HT1, and HT2 films. A pair of bands recognized at 2872 cm^{-1}, and 2823 cm^{-1}, in F, is assumed to be a contribution from the aliphatic -O−CH_3 band attached to FCD structure. But none of these bands were detected in the as-synthesised and heat treated films. The bands seen at 2926 (PF), 2917 (HT1), and 2927 cm^{-1} (HT2) might be due to C–H stretching and correlated to the plasma polymerization of PPFCD films. The C≡C bands detected, in PF and HT1 films, at 2177 and 2202 cm^{-1} are also considered to be formed in plasma polymerization process [43]. The strong absorption peaks identified at 1670–1600 cm^{-1} in all films might be associated with C=C stretching vibrations. Two other absorption bands recorded at 1495 and 1423 cm^{-1} are due to the asymmetric C−H bending. The absorption bands found at 1495 and 1423 cm^{-1} in F, 1558 cm^{-1} in PF, and 1423 cm^{-1} in HT1 films are also assumed to be originated from asymmetric C−H bending while these bands were not seen in HT2 films. The bands seen at 1365–1315 cm^{-1} represent the symmetric C−H bending vibrations of −CH_3 bands. The absorption bands in between 1240 and 1170 cm^{-1} in F, PF, and HT2 films are due to C−C skeletal vibrations. In F, bands seen at 1054, 961, and 754 cm^{-1} indicate the occurrence of respectively C−H in plane bending, C−H rocking, as well as =C−H out-of-plane bending [44]. However, none of these bands were HT1, and HT2 films. This may be happened due to the plasma polymerization and heat treatment effect. Two other strong bands found at 607 cm^{-1}, and 586 cm^{-1} in F, and PF films respectively are

Table 2
Assignments of FTIR absorption peaks for FCD, as- synthesised and heat treated PPFCD samples.

Assignments	Wavenumber (cm^{-1})			
	Monomer	As-deposited	Heat treated PPFCD	
	FCD (F)	PPFCD (PF)	473 K (HT1)	573 K (HT2)
O—H stretching vibration (α)	3154	3380	3354	3439
Asym. C—H stretching (β) (((vibration	–	2926	2917	2927
Aliphatic —O—CH_3 vibration (γ)	2872, 2837	–	–	–
C≡C stretching vibration (δ)	–	2177	2202	–
C=C stretching vibration (ε)	1663	1603	1632	1632
Asym. C—H bending (ζ)	1495, 1423	1558	1423	–
Symmetric C—H bending (θ)	1318	–	1360	1362
C—C skeletal vibration (ι)	1177	1261	–	–
C=H plane bending (κ)	1054	–	–	–
C—H rocking (λ)	961	–	–	–
=C—H out of plane bending (μ)	754	–	–	–
C=C out-of-plane bending (ν)	607	586	–	–

Table 3
Elements detected by EDX in FCD, as- synthesised and heat treated PPFCD thin films.

Sample	Elements detected (wt%)			
	C	O	H	Si
FDH (Calculated from molecular formula)	62.50	33.30	4.20	–
PPFDH (As-deposited with thickness 230 nm)	46.4	34.82	–	18.78
PPFDH (heat treated at 473 K)	51.5	30.42	–	18.08
PPFDH (heat treated at 573 K)	54.84	27.52	–	17.64

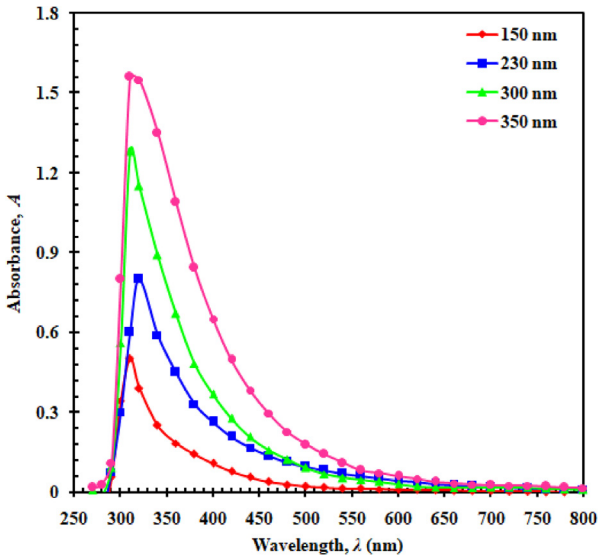

Fig. 8. Variation of *A* with λ for as-deposited PPFCD thin films at different thicknesses.

related to the C=C out of plane bending [34]. A full list of the band frequencies and their corresponding vibrational mode are summarized in Table 2. In all cases, Database Spectrum version 10.4.4 has been used to assign the absorption peaks.

Morphological and compositional analysis of PPFCD films

SEM analysis

The SEM images of the various samples were taken to observe the surface morphology, including surface uniformity, presence of pinholes and fractures in the samples. The SEM images of as-deposited (thickness

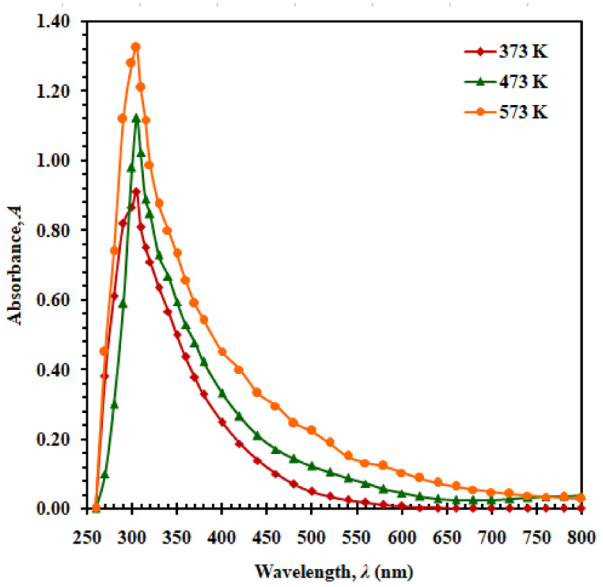

Fig. 9. Variation of *A* with λ for PPFCD thin films heat treated at 373, 473, and 573 K (thickness = 230 nm).

230 nm) as well as heat treated (at temperatures of 373, 473 and 573 K) PPFCD thin films at magnification 50 k × are shown in supplementary section. It is observed from micrographs that the surface of the both as-synthesised and heat treated samples are smooth, homogeneous, pin-hole free and continuous. Henceforth, no remarkable changes in the surface morphological features of the films were observed owing to the heat treatment of the samples up to a temperature, 573 K. The obtained results are well concurred with previous cited results [34,41,45].

EDX analysis

The EDX connected to the scanning electron microscope was performed to figure out the atomic and weight percentage (wt.%) of various elements available in FCD, as synthesised PPFCD as well as heat treated PPFCD films. A complete summary of the EDX analysis of PPFCD films are presented in Table 3. The results obtained from EDX analysis confirmed the presence of carbon (C), oxygen (O) and unwanted silicon (Si) in each thin films samples. Moreover, the results indicated that the C possess the most dominant elements, i.e., maximal wt.% and the amount of O follows a good ratio as it is expected from the chemical structure of the monomer, FCD. The appearance of exceeding wt.% of O in the as-deposited films due to the incorporation of neighbouring O during film handling processes. The reduction of the wt.% of

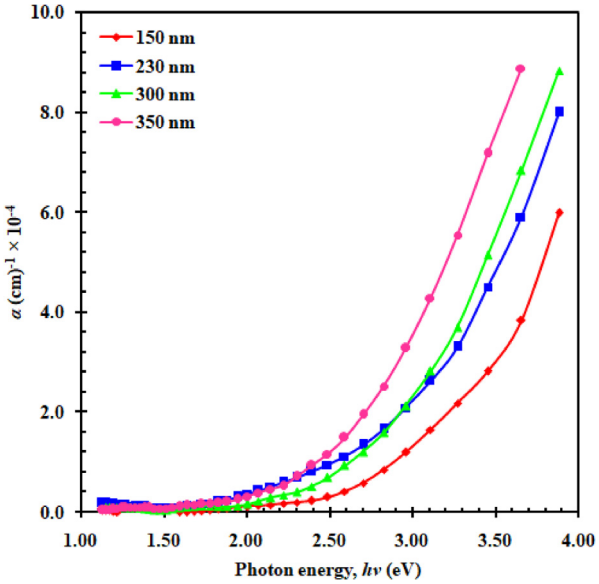

Fig. 10. Change of α with $h\nu$ for as-deposited PPFCD thin films at different thicknesses.

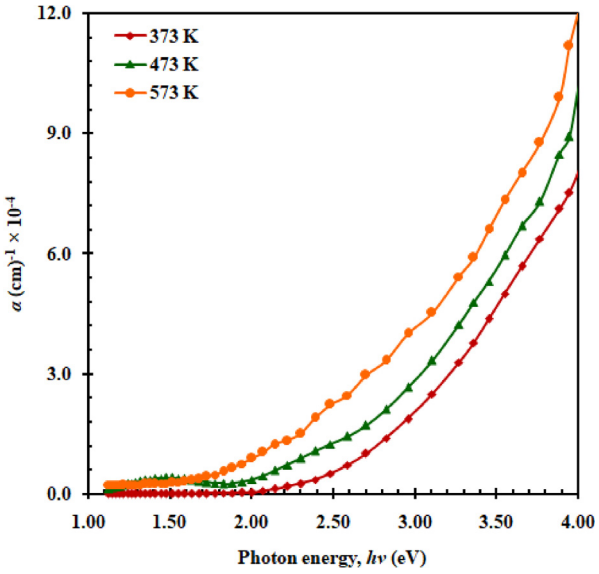

Fig. 11. Change of α with $h\nu$ for PPFCD thin films heat treated at 373, 473, and 573 K (thickness = 230 nm).

O in heat treated PPFCD thin films compared to the as-synthesised PPFCD films may be due to the evolution of O and H from PPFCD thin films as a result of structural rearrangement during heat treatment. Finally, the presence of Si in PPFCD thin films might be originated from the substrate material used in the synthesis process [27].

Optical analysis of PPFCD films

Absorbance and absorption co-efficient

The investigation of the optical absorption spectra is one kind of most efficient approaches for comprehending the energy band diagram of crystalline as well as amorphous materials. In this study, the optical absorption edge was investigated to find out several optical parameters including absorption co-efficient, optical band gap, Urbach energy, etc., for the as-synthesised and heat treated PPFCD films. The UV–Vis absorption spectra of as-synthesised with various thicknesses, and the heat treated at three different temperatures including 373, 473, and 573 K,

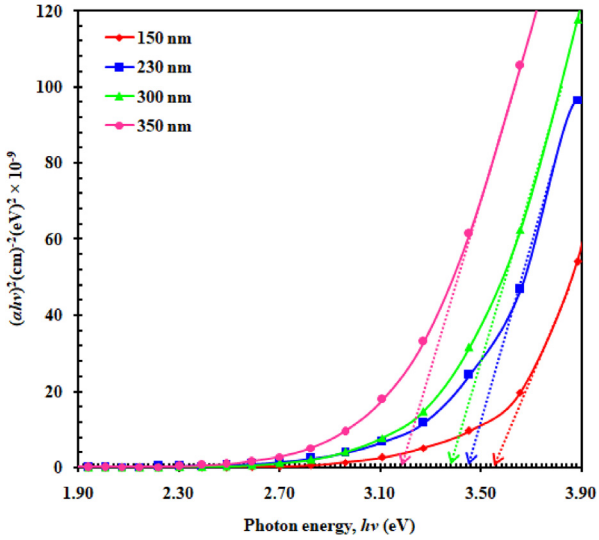

Fig. 12. $(ah\nu)^2$ vs. $h\nu$ curves for as-deposited PPFCD thin films at different thicknesses.

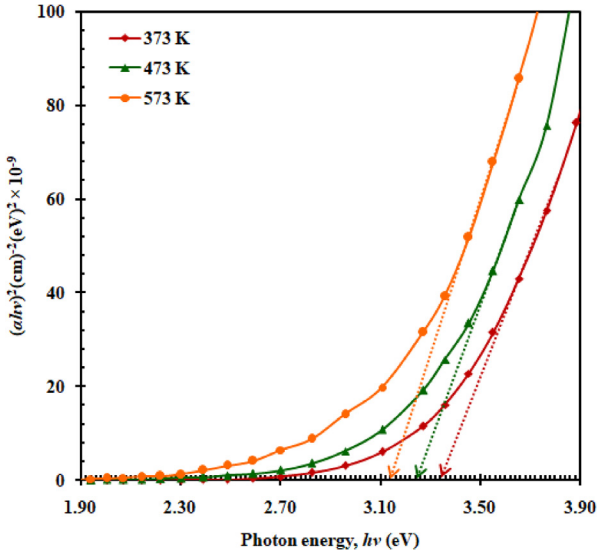

Fig. 13. $(ah\nu)^2$ vs. $h\nu$ curves for PPFCD thin films heat treated at 373, 473, and 573 K (thickness = 230 nm).

of the PPFCD films with a thickness of 230 nm in the wavelength range between 250 and 800 nm are shown respectively in Figs. 8 and 9. The absorption spectra revealed that the entire absorption of the PPFCD films is increased with increasing thickness and heat treatment temperature. Analogous behaviour of optical absorption results of PPFCD films were reported by several authors [40,46].

The absorption coefficient, α, of PPFCD thin films in terms of absorbance (A) and thickness (d) was estimated by the following Eq. (2) [47] ,

$$\alpha = \frac{2.303A}{d} \tag{2}$$

The variation of α, with respect to photon energy ($h\nu$) for as-synthesised (with various d), and heat treated (at several temperatures including 373, 473, and 573 K) PPFCD samples films with a thickness of 230 nm are depicted in Figs. 10 and 11, respectively. Figs. 10 and 11 exhibit the exponential falling edges of α at the lower energy zone and might be appeared due to the short range order and/or the presence of defects in the PPFCD thin film structures [48]. The nature of these absorption coefficient spectra have varied slopes indicating different

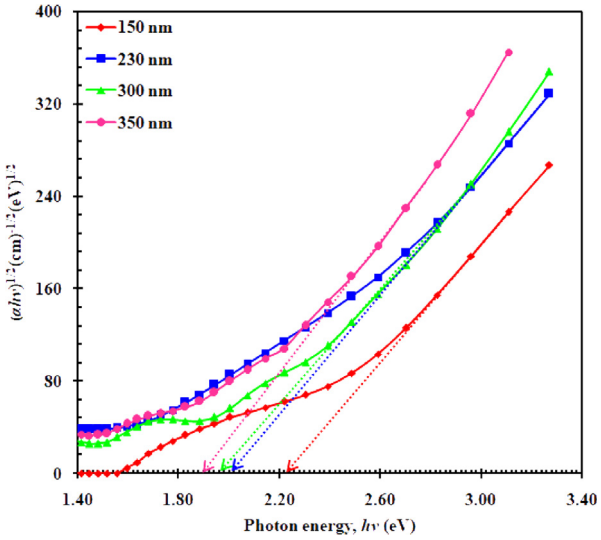

Fig. 14. $(\alpha h\nu)^{1/2}$ vs. $h\nu$ curves for as-deposited PPFCD thin films at different thicknesses.

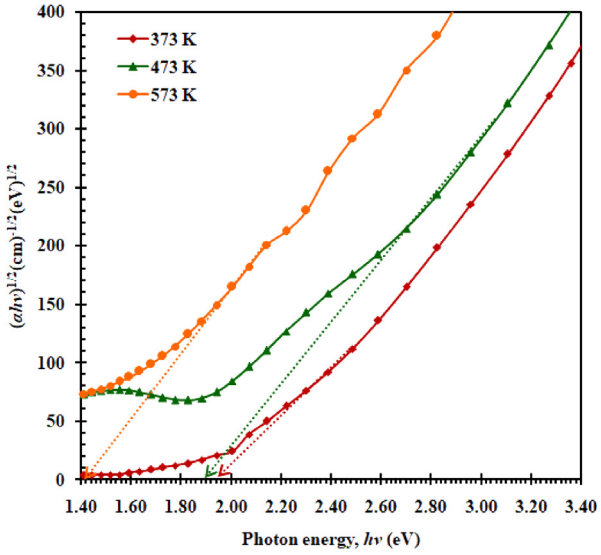

Fig. 15. $(\alpha h\nu)^{1/2}$ vs. $h\nu$ curves for PPFCD thin films heat treated at 373, 473, and 573 K (thickness = 230 nm).

optical transitions involved in PPFCD films. Similar type of observation were found in a variety of organic thin films.

Evaluation and analysis of optical band-gap

In the materials possessing crystalline and amorphous nature, optical transitions *via* photon absorption follows the Tauc relation [49],

$$\alpha h\nu = T(h\nu - E_b)^p \quad (3)$$

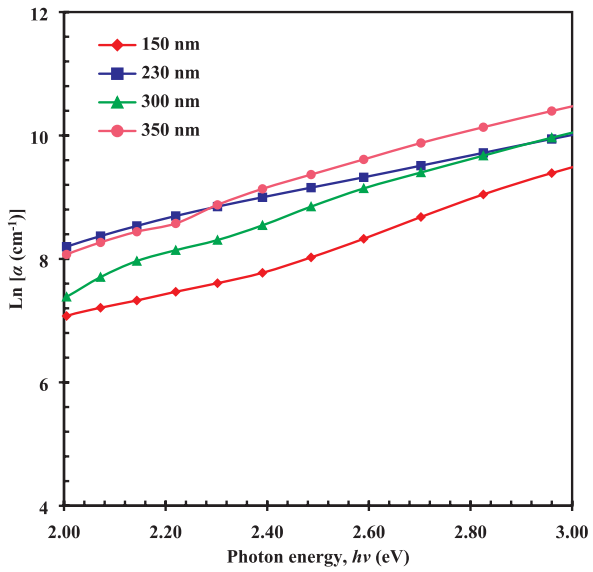

Fig. 16. Ln α vs. $h\nu$ curves for as-deposited PPFCD thin films at different thicknesses.

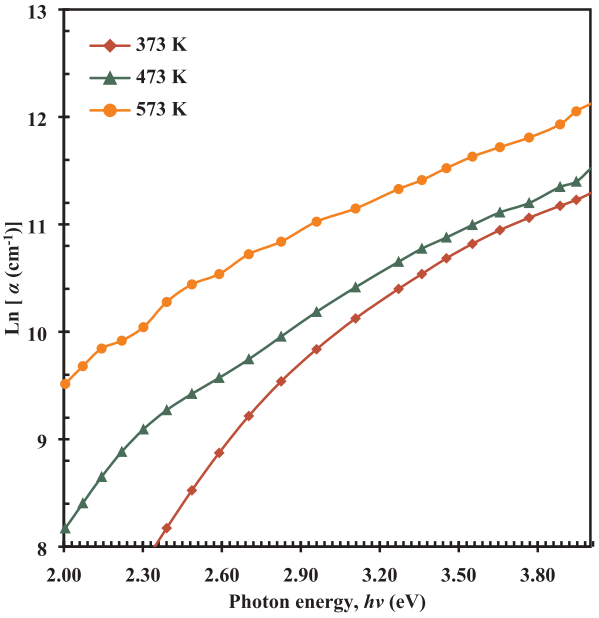

Fig. 17. Ln α vs. $h\nu$ curves for PPFCD thin films heat treated at 373, 473, and 573 K (thickness = 230 nm).

where $h\nu$ indicate the incident photon energy, T is an energy independent parameter called Tauc parameter, E_b is the optical band-gap (OBG) energy and p is an index indicating the nature of optical transitions. The value of p can be assumed 1/2, and 2 respectively for the

Table 4
Values of allowed direct and indirect transition energy gaps for as-synthesised and heat treated (at 373, 473 and 573 K for 1 h) PPFCD thin films.

Film thickness, d (nm)	Direct transition energy gap, E_{db} (eV)				Indirect transition energy gap, E_{ib} (eV)			
	As- synthesised	Heat treated for 1.0 h at (K)			As- synthesised	Heat treated for 1.0 h at (K)		
		373	473	573		373	473	573
150	3.56	–	–	–	2.22	–	–	–
230	3.46	3.36	3.24	3.06	2.00	1.94	1.88	1.42
300	3.38	–	–	–	1.96	–	–	–
350	3.18	–	–	–	1.90	–	–	–

Table 5
Values of Urbach energy and steepness parameter for as-synthesised and heat treated (at 373, 473 and 573 K for 1 h) PPFCD thin films.

Film thickness, d (nm)	Urbach energy, E_U (eV)				Steepness parameter, σ (eV)			
	As- synthesised	Heat treated for 1.0 h at (K)			As- synthesised	Heat treated for 1.0 h at (K)		
		373	473	573		373	473	573
150	0.35	–	–	–	0.0738	–	–	–
230	0.58	0.66	0.78	0.94	0.0446	0.0392	0.0331	0.0275
300	0.42	–	–	–	0.0616	–	–	–
350	0.46	–	–	–	0.0562	–	–	–

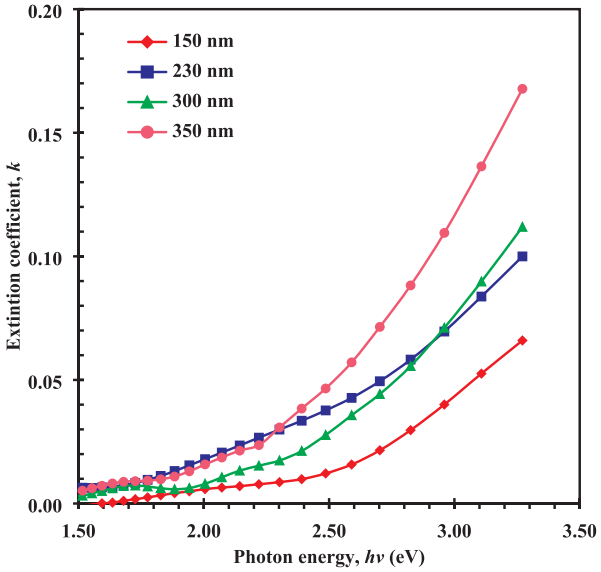

Fig. 18. Variation of k with $h\nu$ for as-deposited PPFCD thin films at different thicknesses.

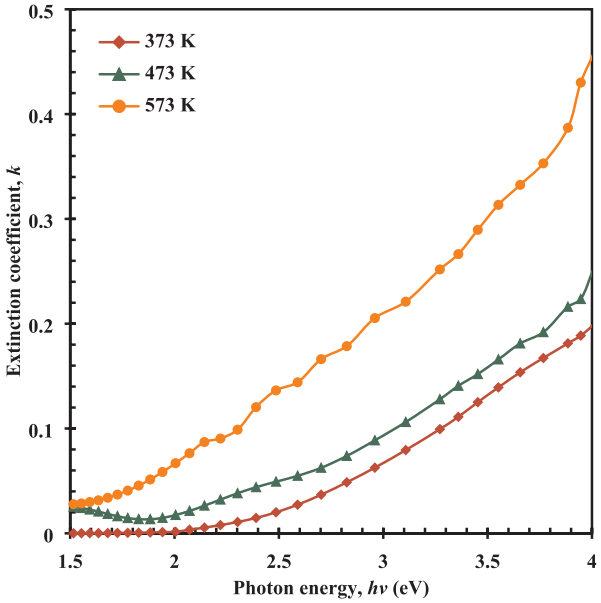

Fig. 19. Variation of k with $h\nu$ for PPFCD thin films heat treated at 373, 473, and 573 K (thickness = 230 nm).

direct and indirect optical transition. The value of E_b can be determined by extrapolating the linear portion of the $(\alpha h\nu)^{1/p}$ against $h\nu$ plot to $h\nu = 0$. The OBG values of PPFCD films were worked out using the Tauc plots of $(\alpha h\nu)^2$ versus $h\nu$, and $(\alpha h\nu)^{1/2}$ vs $h\nu$, respectively. Fig. 12 shows the Tauc plots of $(\alpha h\nu)^2$ versus $h\nu$ for as-synthesised PPFCD thin films with varied thicknesses while that of heat treated with a thickness of 230 nm are presented in Fig. 13. The Tauc plots of $(\alpha h\nu)^{1/2}$ against $h\nu$ for the as-synthesised with various thicknesses and heat treated PPFCD films are displayed in Figs. 14 and 15. The calculated values of direct band-gap, E_{db} and the indirect band-gap, E_{ib} of both sets of PPFCD films are tabulated in Table 4. It is observed from the results shown in Table 4 that the values of both E_{db} and E_{ib} for the as-deposited films decreased slightly with the increase in film thicknesses. This reducing nature of the values of E_{db} and E_{ib} is because of the structural defects in the films occurred during the process of plasma polymerization [35]. Conversely, in the case of heat treated thin films, the values of E_{db} and E_{ib} of PPFCD thin films are monotonically dropped with the gradual enhance in heat treatment temperatures. These declining nature of the values of energy band-gaps for heat treated PPFCD films may appear from the structural rearrangement and/or may be due to the conjugation originated from heat treatment procedures. This results are found to be consistent with a few former investigation [34,36]. Moreover, the estimated values of E_{db} and E_{ib} for both as-synthesised and heat treated PPFCD films are in the range of 3.56–3.00 eV and 2.22–1.32 eV, respectively, and those values imply the amorphous or noncrystalline nature of the PPFCD thin films.

Estimation and analysis of Urbach energy

An exponential tail, called, Urbach spectral tail, in the low crystalline and amorphous materials deals with an exponential part of the absorption coefficient curve closes to the optical band edge. This spectral tail originated from the localized states, and interprets defect states or disorders of the thin films. The Urbach empirical rule for spectral tail analysis can be enunciated by the subsequent relation [50],

$$\alpha = \alpha_o exp(h\nu/E_U) \quad (4)$$

where α_o is a constant while E_U indicates Urbach energy, and is weakly influenced by temperature. In fact, Urbach edge is an excellent way to evaluate the disorderness of thin films materials. Taking logarithm of both sides of Eq. (4), we have the following equation:

$$ln\alpha = ln\alpha_o + (h\nu/E_U) \quad (5)$$

Therefore, Urbach energy can be computed from the gradient of the lnα versus $h\nu$ plot. Fig. 16 represents the Urbach energy plot for as synthesised PPFCD thin films with varying thicknesses, whereas same plot for heat treated PPFCD thin films samples are illustrated in Fig. 17, and obtained values of Urbach energy is presented in Table 5. It is observed that the values of Urbach energy increase with increasing both thickness of the PPFCD films and temperature of the heat treatment process. This behavior might be due to the enhancement of the disorderness as well as density of defect states around the PPFCD films. Similar results were also observed by several researchers [40].

The fluctuation of α with $h\nu$ correlated with the electronic transitions reduces exponentially with $h\nu$ and that is why Eq. (4) can be re-written as [51],

$$\alpha = \alpha_o exp(\sigma(E)/kT) \quad (6)$$

where the symbol σ is steepness parameter, and is related to the broadening of the absorption edge. If the broadness of the absorption edge is associated with the tangent of Eq. (4), the steepness parameter in terms of Boltzmann constant (k_B) can be attained by the succeeding equation [52]:

$$\sigma = k_B T / E_U) \quad (7)$$

The different values of steepness parameter for as synthesised PPFCD films with various thicknesses and heat treated (at several temperatures including 373, 473, and 573 K) PPFCD thin films with a thickness of 230 nm are compiled in Table 5. The results indicates that the values of steepness parameter decrease with increasing both thickness of the PPFCD films and heat treatment temperature. The extinction coefficient, denoted by k, is associated with absorption coefficient and wavelength by the relation as follows [53],

$$k = \alpha\lambda/4\pi) \quad (8)$$

The dependence of k as a function of photon energy for as synthesised PPFCD films and heat treated (at several temperatures including 373, 473, and 573 K) PPFCD thin films with a thickness of 230 nm are plotted in Figs. 18 and 19, respectively. It is observed from Figs. 18 and 19 that the k values are gradually raised with respect to the $h\nu$ for both as synthesised and heat treated PPFCD thin films. This nature of k relating to the $h\nu$ exhibits the possibility of electron movement across the mobility gap [54]. Moreover, the least possible k values in the visible spectral region ascertained that the as synthesised and heat treated PPFCD film are quite suitable for the application of optical devices, such as lenses and anti-reflection coatings [25,55,56].

Conclusions

The uniform and fracture free amorphous PPFCD thin films with thicknesses of 150–350 nm were successfully prepared with the plasma assisted glow discharge technique. From the structural and morphological investigations, we see that there was no significant influence on the amorphous characteristics of PPFCD films and the film structures are thermally stable up to 600 K. Because of plasma polymerization and heat treatment effect, the functional groups such as C—H plane bending, C—H rocking, and ═C—H out-of-plane bending were not seen in the as-synthesised and heat treated PPFCD films. The reduction in the wt.% of O in the heat treated PPFCD thin films compared to those of as-synthesised films might be occurred due to the evolution of O and H from the film surfaces in the heat treatment process. The direct and indirect optical band-gap energies of both as-synthesised and heat treated PPFCD thin films were found to be gradually reduced with the successive increment of the film thickness and heat treated temperatures. The Urbach energy of the PPFCD thin films was found to be enhanced with increasing temperature of the heat treatment process, while reverse results was observed for Steepness parameter.

Declaration of Competing Interest

The authors declare that they have no known competing financial interests or personal relationships that could have appeared to influence the work reported in this paper.

Acknowledgements

This work was financial supported by the Bangladesh University of Engineering and Technology (BUET). H Kabir and M M Rahman are grateful to Jahangirnagar University for providing with the logistic supports to carry out this project.

Appendix A. Supplementary data

Supplementary data to this article can be found online at https://doi.org/10.1016/j.rinp.2020.103014.

References

[1] Inagaki N, Kondo S, Hirata M, Urushibata H. Plasma polymerization of organosilicon compounds. J Appl Polym Sci 1985;30(8):3385–95.
[2] Easton CD, Jacob MV. Ageing and thermal degradation of plasma polymerised thin films derived from Lavandula angustifolia essential oil. Polym Degrad Stab 2009;94(4):597–603.
[3] Bao S, Yamada Y, Okada M, Yoshimura K. The effect of polymer coatings on switching behavior and cycling durability of Pd/Mg–Ni thin films. Appl Surf Sci 2007;253(14):6268–72.
[4] Zhao X, Wang M, Xiao J. Deposition of plasma conjugated polynitrile thin films and their optical properties. Eur Polym J 2006;42(9):2161–7.
[5] Nasrin R, Bhuiyan A. Evaluation of electrical carrier transport mechanism in plasma polymerized n -butyl methacrylate thin films. Polym Phys Ser A 2018;60(6):886–93.
[6] Anderson L, Jacob M. Effect of RF power on the optical and morphological properties of RF plasma polymerised linalyl acetate thin films. Appl Surf Sci 2010;256(10):3293–8.
[7] Yasuda H. Glow discharge polymerization. J Polym Sci Macromol Rev 1981;16(1):199–293.
[8] Shi FF. Recent advances in polymer thin films prepared by plasma polymerization Synthesis, structural characterization, properties and applications. Surf Coat Technol 1996;82(1):1–15.
[9] Lakshmi GBVS, Dhillon A, Siddiqui AM, Zulfequar M, Avasthi DK. RF-plasma polymerization and characterization of polyaniline. Eur Polym J 2009;45(10):2873–7.
[10] Kabir H, Bhuiyan AH, Rahman MM. Understanding the charge carrier conduction mechanisms of plasma-polymerized 2-furaldehyde thin films via DC electrical studies. Thin Solid Films 2016;609(C):35–41.
[11] Utracki LA, Plasma deposition, treatment, and etching of polymers edited by R. d'Agostino Academic Press, Inc., Boston 528 pages, hard cover, 1990, 1993, pp. 385–390.
[12] Riveros G, Baez C, Ramírez D, Pereyra CJ, Marotti RE, Romero R, et al. Electrodeposition and characterization of composition-graded CdSxSe(1–x) multilayer thin film structures. J Alloy Compd 2016;686:235–44.
[13] Santhosh TCM, Bangera KV, Shivakumar GK. Band gap engineering of mixed Cd (1–x)Zn (x) Se thin films. J Alloy Compd 2017;703:40–4.
[14] Zhou ZB, Cui RQ, Pang QJ, Hadi GM, Ding ZM, Li WY. Schottky solar cells with amorphous carbon nitride thin films prepared by ion beam sputtering technique. Sol Energy Mater Sol Cells 2002;70(4):487–93.
[15] Rahman M, Jiang Z-T, Munroe P, Chuah L, Zhou Z-F, Xie Z, et al. Chemical bonding states and solar selective characteristics of unbalanced magnetron sputtered $Ti_xM_{1-x-y}N_y$ films. RSC Adv 2016;6(43):36373–83.
[16] López J, Solorio E, Borbón-Nuñez HA, Castillón FF, Machorro R, Nedev N, et al. Refractive index and bandgap variation in Al2O3-ZnO ultrathin multilayers prepared by atomic layer deposition. J Alloy Compd 2017;691:308–15.
[17] Mukherjee A, Fu M, Mitra P. Influence of Zn incorporation in CdS: structural and morphological studies. J Phys Chem Solids 2015;82:50–5.
[18] Rossi D, Schreiner WH, Durrant SF. Characterization of amorphous hydrogenated chlorinated plasma polymers. Surf Coat Technol 2016;289:118–23.
[19] Jacob MV, Olsen NS, Anderson LJ, Bazaka K, Shanks RA. Plasma polymerised thin films for flexible electronic applications. Thin Solid Films 2013;546(C):167–70.
[20] Moosburger-Will J, Bauer M, Schubert F, Kunzmann C, Lachner E, Zeininger H, et al. Methyltrimethoxysilane plasma polymerization coating of carbon fiber surfaces. Surf Coat Technol 2017;311:223–30.
[21] Sarker RB, Bhuiyan AH. Electrical conduction mechanism in plasma polymerized 1-Benzyl-2-methylimidazole thin films under static electric field. Thin Solid Films 2011;519(18):5912.
[22] Nasrin R, Bhuiyan A. Thermal and AC electrical properties of thin films prepared from n-BUTYL methacrylate by a capacitively coupled plasma reactor. J Surf Rev Lett 2019;26(02):1850146.
[23] Amri A, Hasan K, Taha H, Rahman MM, Herman S, Andrizal E, et al. Surface structural features and optical analysis of nanostructured Cu-oxide thin film coatings coated via the sol-gel dip coating method. Ceram Int 2019;45(10):12888–94.
[24] Martin L, Esteve J, Borrós S. Growth vs. nucleation of conducting polymers thin films obtained by plasma-enhanced chemical vapor deposition. Thin Solid Films 2004;451:74–80.
[25] Banu N, Bhuiyan AH, Hossain KS. Characterization of structural and optical properties of plasma polymerized diethanolamine thin films. Adv Polym Technol 2018;37(8):3084–94.
[26] Rahman MM, Jiang Z-T, Zhou Z-F, Xie Z, Yin CY, Kabir H, et al. Effects of annealing temperatures on the morphological, mechanical, surface chemical bonding, and solar selectivity properties of sputtered TiAlSiN thin films. J Alloy Compd 2016;671(C):254–66.
[27] Kabir H, Rahman MM, Uddin KM, Bhuiyan AH. Structural, morphological, compositional and optical studies of plasma polymerized 2-furaldehyde amorphous thin films. Appl Surf Sci 2017;423:983–94.
[28] Rahman M, Bhuiyan A. AC electrical properties of plasma polymerized o -methoxyaniline thin films. Polym Phys 2018;60(3):290–7.
[29] Afroze T, Bhuiyan AH. Thickness dependence of ac electrical conductivity and dielectric behavior of plasma polymerized 1, 1, 3, 3–tetramethoxypropane thin films. Polym Eng Sci 2018;58(8):1342–5.
[30] Islam S, Hossain M, Kabir H, Rahaman M, Bashar M, Gafur M, et al. Optical, structural and morphological properties of spin coated copper zinc tin sulfide thin

films. J Int J Thin Films Sci Technol 2015;4(3):155.
[31] Nasrin R, Hossain K, Bhuiyan A. Morphological, elemental, and optical characterization of plasma polymerized n -butyl methacrylate thin films. Appl Phys A 2018;124(5):1–8.
[32] Kabir H, Rahman MM, Roy TS, Bhuiyan A. Structural and optical properties of plasma polymerized pyromucic aldehyde thin films. Int J Mech Mechatron Eng 2012;12(5):30–4.
[33] Das SK, Islam JM, Hasan M, Kabir H, Gafur MA, Hoque E, et al. Astronomy Development of electrically conductive nanocrystalline thin film for optoelectronic applications. Int Lett Chem Phys Astron 2013;10:90–101.
[34] Afroze T, Bhuiyan AH. Effect of aging on the optical properties of plasma polymerized 1,1,3,3-tetramethoxypropane thin films. Adv Polym Technol 2013;32(2):21347.
[35] Matin R, Bhuiyan AH. Heat treatment and aging effect on the structural and optical properties of plasma polymerized 2,6-diethylaniline thin films. Thin Solid Films 2012;520(21):6463–70.
[36] Nasrin R, Bhuiyan A. Effect of heat treatment on infrared and ultraviolet–visible spectroscopic studies of the PPnBMA thin films. Appl Phys A 2018;124(12):1–9.
[37] Kabir H, Nasrin R, Hasan K, Rahman MM, Bhuiyan AH. Synthesis and aging effect of plasma-polymerized 2-furancarboxaldehyde amorphous thin films. Mater Chem Phys 2019;232:209–20.
[38] Matin R, Bhuiyan AH. Effect of iodine doping on the electrical transport mechanism in plasma polymerized 2,6-diethylaniline thin films. J Phys Chem Solids 2014;75(2):198–202.
[39] Majumder S, Bhuiyan A. Effect of heat treatment on the optical properties of plasma-polymerized vinylene carbonate thin films. Adv Polym Technol 2015;34(1):21468.
[40] Momin M, Hossain K, Bhuiyan A. Microstructural, compositional, topological and optical properties of plasma polymerized cyclohexane amorphous thin films. J Polym Res 2019;26(3):1–10.
[41] Tolansky S. Mehrfachreflex-Interferometrie an oberflächen und schichten. Phys J 1948;4(11–12):472–80.
[42] Kaniappan K, Latha S. Certain investigations on the formulation and characterization of polystyrene/poly(methyl methacrylate) blends. Int J ChemTech Res 2011;3(2):708–15.
[43] Scheinmann F, An introduction to spectroscopic methods for the identification of organic compounds, [1st ed.]. ed., Pergamon Press, Oxford, 1970.
[44] Banwell CN, McCash EM. Fundamentals of molecular spectroscopy. 4th ed. London: McGraw-Hill; 1994.
[45] Rahman MJ, Bhuiyan AH. Structural and optical properties of plasma polymerized o-methoxyaniline thin films. Thin Solid Films 2013;534:132–6.
[46] Chowdhury FUZ, Bhuiyan AH. An investigation of the optical properties of plasma-polymerized diphenyl thin films. Thin Solid Films 2000;360(1–2):69–74.
[47] Shah Jalal ABM, Ahmed S, Bhuiyan AH, Ibrahim M. UV-Vis absorption spectroscopic studies of plasma-polymerized m-xylene thin films. Thin Solid Films 1996;288(1–2):108–11.
[48] Akther H, Bhuiyan AH. Electrical and optical properties of plasma-polymerized n , n ,3,5-tetramethylaniline thin films. New J Phys 2005;7(1):173.
[49] Tauc J, Menth A, Wood DL. Optical and magnetic investigations of the localized states in semiconducting glasses. Phys Rev Lett 1970;25(11):749–52.
[50] Urbach F. The long-wavelength edge of photographic sensitivity and of the electronic absorption of solids. Phys Rev 1953;92(5):1324.
[51] Tauc J. Amorphous and Liquid Semiconductors. New York: Plenum Press; 1974.
[52] Fayek SA, Balboul MR, Marzouk KH. Optical, electrical and thermal studies on $(As_2Se_3)_{3-x}(As_2Te_3)x$ glasses. Thin Solid Films 2007;515(18):7281–5.
[53] Al-Ramadin Y. Optical properties of poly(vinyl chloride)/poly(ethylene oxide) blend. Opt Mater 2000;14(4):287–90.
[54] Saturi B, Abdullah C, Fouziah Md Y. Study on optical properties of tin oxide thin film at different annealing temperature. J Sci Technol 1970;4(1):61–72.
[55] Caglar Y, Ilican S, Caglar M. Single-oscillator model and determination of optical constants of spray pyrolyzed amorphous SnO 2 thin films. Condens Matter Complex Syst 2007;58(3):251–6.
[56] Dabbabi S, Nasr TB, Ammar S, Kamoun N. Synthesis and characterization of zinc-tin-mixed oxides thin films. Superlattices Microstruct 2018;123:129–37.